Journal of Institute of Science and Technology, 30(1), 101-113 (2025)
ISSN: 2467-9062 (print), e-ISSN: 2467-9240
https://doi.org/10.3126/jist.v30i1.74723

Research Article

Sesamum Indicum LEAF EXTRACT AS ENVIRONMENTALLY BENIGN INHIBITOR TO MITIGATE MILD STEEL CORROSION IN CEMENT PORE SOLUTION

Madhab Gautam[1,2], Nootan Prasad Bhattarai[1*], Jagadeesh Bhattarai[1*]
[1]*Central Department of Chemistry, Institute of Science and Technology, Tribhuvan University, Kirtipur 44613, Kathmandu, Nepal*
[2]*Department of Chemistry, Tribhuvan Multiple Campus, Tansen 32500, Palpa, Nepal*
**Correspondence: bhattarai_05@yahoo.com; nootan.bhattarai@cdc.tu.edu.np*

(Received:** March 03, 2025; **Final Revision:** March 24, 2025; **Accepted:** April 04, 2025**)

ABSTRACT

Concrete is one of the most widely used building materials after water due to its exceptionally high compressive strength. However, mild steel-reinforced concrete (MSRC) structures often encounter the problem of premature corrosion of the reinforcement. This issue emphasizes the importance of developing effective strategies to mitigate corrosion using inhibitors and understanding corrosion-controlling mechanisms. This work evaluates the effectiveness of *Sesamum indicum* leaf extract (SILE) as an environmentally friendly corrosion inhibitor in a saturated lime water solution with a pH of approximately 12, which simulates a cement pore solution (CPS). For the aim, weight loss (WL) and polarization procedures were conducted over 4 months to assess the corrosion inhibitory ability of SILE at concentrations of 500, 1000, 2000, and 4000 ppm in CPS to mitigate embedded mild steel (EMS) corrosion at a laboratory temperature of 25°C. The maximum inhibition efficiency was observed at 4000 ppm SILE, achieving 93.9% and 81.7% inhibition rates as determined by WL and potentiodynamic polarization (PDP) techniques, respectively. Also, PDP studies revealed a decline in corrosion current density with increasing SILE concentrations, indicating its inhibitory action. By facilitating adsorption onto the EMS surface, secondary metabolites (SMs), like mostly the flavonoids, including polyphenols, alkaloids, and terpenoids in SILE, can impede cathodic, anodic, or both processes. White light interferometry (WLI) and scanning electron microscopy with energy-dispersive X-ray spectroscopy (SEM/EDX) images supported the results of corrosion-inhibiting effectiveness of SILE to improve the corrosion-resistant properties of concrete by the development of passive layer on EMS.

Keywords: Adsorption film, corrosion inhibitor, polarization, reinforcement corrosion

INTRODUCTION

Nowadays, mild-steel reinforced concrete (MSRC) structures are employed extensively in urbanization scenarios worldwide. Concrete alone has to withstand load capacity (Gagg, 2014) and reinforcing mild steel or steel in the concrete increases tensile strength. For example, an ordinary concrete beam without reinforcement possesses a tensile strength of approximately one-tenth of the steel-reinforced concrete beam, totaling around 2-5 MPa. In contrast, the steel-reinforced concrete beam demonstrates considerable tensile strength ranging from 20 to 40 MPa (Jagadesh *et al.*, 2021). Besides, MSRC structures are made more durable by the high alkalinity nature of their pores (i.e., concrete pore solution), which forms a passive diffusion film as cement hydration products that stick to EMS in concrete structures (Jabed *et al.*, 2023). The corrosion problem of MSRC is the early breakdown of EMS (Keles *et al.*, 2023). Chloride, carbon dioxide, sulfur dioxide, and other pollutant gases catalyze the dissolution of passive films by lowering concrete pores' pH with the expansion of reinforcement steel, which causes cracking and spalling with weakening of structures and finally collapsing in aggressive coastal and industrial environments (Fuhaid & Niaz, 2022).

This type of corrosion managed to control, even though it has not stopped (Bhattarai, 2010). Formulation of plant-based eco-friendly inhibitors is one of the best methods to lessen the corrosion problem of MSRC (Giri *et al.*, 2023). Researcher usage of such eco-friendly inhibitors is crucial because most synthetic inorganic and organic inhibitors are banned due to their toxicity (Abdel-Karim & El-Shamy, 2022). Because plant-based inhibitors are inexpensive, non-toxic, and environmentally benign, they make excellent substitutes (Zakeri *et al.,* 2022). Heteroatoms, aromatic rings, and conjugated π-systems are the typical functional groups that permit physical or chemical adsorption to the reinforcing mild steel, preventing corrosion by blocking hostile ions (Hau & Huong, 2022).

Research on preventing early corrosion of the MSRC structures has increased recently, with the addition of plant-based green inhibitors as concrete admixtures (Deyab & Mohsen, 2023). The various studies focus on plant waste components like leaves, bark, fruits, peels, and flowers as concrete admixtures acting as corrosion inhibitors (Bhattarai *et al.*, 2021). Ongoing efforts continue to seek new and more effective green inhibitors for the MSRC structures (Harb *et al.*, 2020), which have almost the same electrolytic environment as the simulated cement pore solution (CPS) from the saturated $Ca(OH)_2$ solution with around 12 pH (Maeda *et al.*, 2020). The need to create environmentally friendly inhibitors to satisfy market needs and replace costly,

hazardous alternatives is growing as green chemistry becomes valuable (Somai *et al.*, 2023). The expanding market for green inhibitors also offers potential economic benefits by developing new plant-based concrete corrosion inhibitors on an industrial scale. Many Nepalese plants remain unexplored in this distinct context, although few studies focused on Nepalese plants as corrosion inhibitors in biofuels (Amagain *et al.*, 2022). Therefore, the leaf extract of an annual, self-pollinating herbaceous plant of *Sesamum indicum* L., referred to as sesame or TIL in Nepali, is explored as a green-based corrosion inhibitor to control premature MSRC corrosion in simulated CPS.

Sesamum indicum L. is a member of the Pedaliaceae family and is widely grown for its seeds and oil because of its high nutritional content (Wu *et al.*, 2019). Therefore, the leaf extract of an annual, self-pollinating herbaceous plant *Sesamum indicum* L. (referred to as sesame or TIL in Nepali), was explored as a green-based corrosion inhibitor to control the premature MSRC corrosion in simulated CPS. *Sesamum indicum* L. is an annual, self-pollinating herbaceous plant from the Pedaliaceae family. It is extensively cultivated for its seeds and oil due to its high nutritional value (Wu *et al.*, 2019). Sesame, a native of Africa and Asia, is regarded as one of the earliest oilseed crops in human history and has been known since 1600 BC (Nagendra *et al.*, 2012). The plant has an erect, pubescent stem ranging from 0.60 to 1.20 meters in height, with ovate to lanceolate leaves that vary in shape along the stem (Mukta & Neeta, 2017). Often referred to as the "Queen of oilseed crops," sesame seeds are valued for their high oil yield, stable quality, and resistance to rancidity in hot climates (Narasimhan & Mohan, 2012).

Historically, sesame was used in traditional Chinese and Indian medicine for pain relief, anti-aging properties, and energy enhancement, highlighting its pharmacological importance (Mukta & Neeta, 2017). Phytochemical analysis of *Sesamum indicum* L. leaf extract reveals the presence of alkaloids, flavonoids, polyphenols, sterols, terpenoids, glycosides, carbohydrates, and proteins. At the same time, sesame oil contains lignans like sesamin, sesamol, and sesamolin, along with acyl glycerols such as oleic, linoleic, palmitic, stearic, and arachidic acids, contributing to its unique properties (Wei *et al.*, 2022). Gravimetric and linear polarization methods studied corrosion inhibiting action of steam and leaf extracts for MS in 2M HCl and H_2SO_4 solutions, proving effective in preventing corrosion in acidic environments (Popoola *et al.*, 2012). Additionally, sesame oil has been reported to inhibit the corrosion of MS in saline solutions (Oyekunle, 2019).

In such possibilities, the author explores a distinctive approach by investigating the ability of methanolic leaf extract of *Sesamum indicum L.* (SILE) to prevent corrosion in a simulated CPS with an alkaline pH around 12, similar to that of reinforced concrete. The primary objective is to assess the long-term anti-corrosive efficacy of methanolic SILE as a corrosion inhibitor in cement pore solutions prepared using a calcium hydroxide [$Ca(OH)_2$] solution, which approximates the desired pH level. The study operates two main techniques: potentiodynamic polarization (PDP) and weight loss (WL) analysis to evaluate the effectiveness of SILE in preventing MS corrosion in CPS. Furthermore, surface analyses, including two-dimensional (2D) SEM/EDS and three-dimensional (3D) WLI used to support the findings from the WL and PDP methods. The results of this research contribute valuable insights for devising eco-friendly concrete admixtures from the leaf extract of the *Sesamum indicum L.*

MATERIALS AND METHODS

Sesamum indicum L. leaves (Fig. 1a) were collected from Pigaunna-2, Mahottari-Nepal, and confirmed at the Department of Plant, National Herbarium and Plant Laboratory in Godavari, Lalitpur. They were kept in shaded areas, dried, and pulverized using an electric mill (Fig. 1b), and steeped in a 1:2 methanol solution for two weeks while stirred frequently (Fig. 1c). The supernatant was next filtered and evaporated at 40°C with a rotary evaporator (IKA® RV 10 digital V, Germany), as shown in Fig. 1(d), to create a semi-solid form of plant extracts, as previously described (Giri *et al.*, 2023). A semi-solid *Sesamum indicum* extract (SILE) was kept at 4°C. After that, a saturated $Ca(OH)_2$ solution with a pH of around 12 was employed to make the simulated CPS. The chemicals used in this study are methanol (CAS No.: 67-56-1) and calcium carbonate (CAS No.: 471-34-1, ADR/PG), procured from Thermo Fisher Scientific India Pvt. Ltd. and LOBA CHEME Pvt. Ltd., respectively, with a purity of ≥98%.

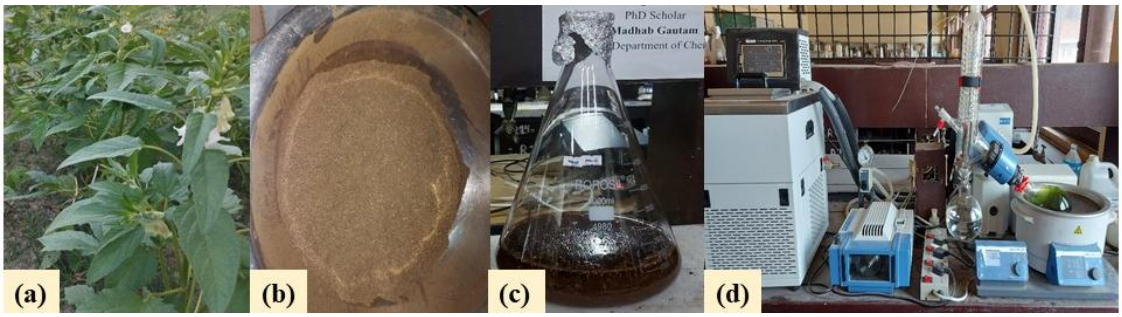

Figure 1. Photographs showing different steps for preparing extract: (a) leaves of *Sesamum indica* L. plant, (b) pulverized leaf powder, (c) soaked with methanol, and (d) rotary evaporator for evaporation of solvent

Fifteen fresh and rust-free mild steel rebar specimens (the company's name was kept anonymous for ethical issues), designated as the 500 XD series (abbreviated as 500MS), were prepared for the weight loss technique to estimate the corrosion rate, as detailed in literature (Subedi *et al.*, 2019). Each 500MS specimen had an average diameter of 11.3 mm and a length of approximately 20 mm. Initially, the weight of each 500MS specimen (denoted as W_i) was recorded meticulously using a 5-digit micro-balance (BM-252; A&D Weighing Company, Japan), which has an accuracy of 0.00001 grams and is available at the laboratory of the Department of Environment-Nepal Government. The weight composition of the 500MS rebar is approximately 98% iron (Fe), with small amounts of carbon (C), manganese (Mn), sulfur (S), and phosphorus (P), as described in Gautam *et al.* (2024a).

Three 500MS specimens, among the 15, were submerged in 100 mL beakers containing 50 mL of CPS without plant extract (control CPS). The remaining 12 specimens were dipped individually into three 100 mL beakers, each containing 50 mL of CPS with varying concentrations of SILE (500, 1000, 2000, and 4000 ppm) over approximately four months (2802 hours). The 500MS specimens underwent regular weight measurements (denoted as W_f) using a digital micro-balance at 7, 14, 28, 43, 60, 90, and 118 days while exposed to each CPS variant. Subsequently, the corrosion rate (CorR) for each specimen in both the controlled CPS and CPS with SILE concentrations ranging from 500 to 4000 ppm was calculated, along with the corrosion inhibition efficiency (CorIE), using the formula provided in equation (1) (Rana *et al.*, 2017). Furthermore, surface coverage (θ) and percentage inhibition efficiency (%IE), determined from the corrosion rates in the control solution ($CoR_{con.}$) and the extract-treated CPS ($CoR_{inh.}$), applying the equations (2) and (3), respectively. The weight loss (Δw) was calculated using equation (4).

$$CorR_{con./Inh.}\ (mm/y) = \frac{\Delta W\ (g) \times 87600}{A\ (cm^2) \times \varrho\ (gcm^{-2}) \times t\ (hrs.)} \quad (1)$$

$$\theta = \frac{CorR_{con.} - CorR_{inh.}}{CorR_{con.}} \quad (2)$$

$$\%IE\ (\%) = \frac{CorR_{con.} - CorR_{inh.}}{CorR_{con.}} \times 100 \quad (3)$$

$$\text{Where, } \Delta W = W_i - W_f \quad (4)$$

In addition, an electrochemical investigation carried out using a potentiostat with a three-electrode system (Iquant 64; Model No.: IFC 101-32240) for potentiodynamic polarization (PDP) studies, as previously described (Gautam *et al.*, 2024b). During this process, the corrosion potential (E_{cor}), corrosion current density (i_{cor}), corrosion rate (CorR) based on i_{cor}, or $CorR_{icor}$, and inhibition efficiency (IE) based on i_{cor}, or IE_{icor} were calculated from the slopes of the anodic and cathodic polarization curves using formulas (5) and (6) (Gautam *et al.*, 2024a). Therefore, Tafel plots of the anodic and cathodic curves extended to determine $CorR_{icor}$ and IE_{icor} (Magrati *et al.*, 2020).

$$CorR_{icor} = 0.13 \times i_{corr} \times \frac{E}{\varrho} \quad (5)$$

$$IE_{icor}\ (\%) = \frac{icor_{con.} - icor_{inh.}}{icor_{con.}} \times 100 \quad (6)$$

Where, ϱ = 7.86 g/cm³, is density and E = 55.85, equivalent weight of steel specimens.

Furthermore, two types of adsorption isotherm models (Langmuir and Temkin) are applied to explain the inhibitory activity of secondary metabolites present in the SILE (plant extract) using the linear fit plots of both the isotherms, as displayed in equations (7) and (8), respectively, for Langmuir adsorption linear fit (Langmuir, 1916) and Temkin adsorption linear fit (Temkin, 1941).

$$\frac{C_{SILE}}{\theta} = \frac{1}{K_{ads}} + C_{SILE} \quad (7)$$

$$\theta = B_{Tem} \log (KE_{Tem}) + B_{Tem} \log (C_{SILE}) \quad (8)$$

Where K_{ads} is equilibrium constant for adsorption, which assists in calculating the free energy change of adsorption (ΔG_{ads}), and can be calculated heat of adsorption (ΔH_{ads}) with the help of the B_{Tem}, as described in literature (Gautam *et al.*, 2024b)

The FT-IR spectra were obtained from the ATR method using an IR Affinity-1S instrument (Shimadzu Corp., Japan) in the wave number between 400 and 4000 cm^{-1} with a scan speed of 16 scans per second to identify the functional groups present in SILE. In addition to the FT-IR analysis, phytochemical experiments were conducted on SILE to determine the presence (+) or absence (−) of various secondary metabolites, as described elsewhere (Gautam *et al.*, 2025). A scanning electron microscope (Thermo Fisher Scios Field Emission, USA, 10 kV), coupled with an energy dispersive X-ray spectroscopy (EDAX Octane Elect EDS/EDX detector, USA, 30 kV), was utilized to analyze the two-dimensional morphological and compositional changes of the 500MS specimens after 2802 hours of immersion in CPS, both with and without SILE at concentrations ranging from 500 to 4000 ppm. Employing white light interferometry-WLI (NewView-9000, Zygo Corporation) to assess surface roughness and create three-dimensional (3D) images of the 500MS specimens immersed in CPS, both without and with SILE. Also, the characteristic phyto-compounds of the SILE were identified using liquid chromatography-mass spectrometer (LC-MS, Water Corp., USA) using a high-performance quadruple time-of-flight mass spectrometer (XEVO G2-XS QTOF) at IIT Ropar, Punjab.

RESULTS AND DISCUSSION

Qualitative chemical tests for SMs of SILE were performed from the chemical screening tests, as

described elsewhere (Gautam *et al*., 2025), and Table 1 presented the experimental outcomes of the chemical screening tests. Flavonoids, alkaloids, terpenoids, steroids, phenolics, saponins, and glycosides are compounds that contain significant amounts of heteroatoms such as nitrogen (N) and oxygen (O), as well as unsaturated electrons and/or aromatic systems (Fuji *et al*., 2018).

Table 1. Qualitative chemical tests for secondary metabolites (SMs) in SILE

SMs	Alkaloid	Phenol	Flavonoid	Glycoside	Saponin	Tannin	Terpenoid	Steroid	Carbohydrate
SILE	+++	++	+++	+	++	++	+++	+++	–

('+' or '++' or '+++' sign refers to presence with abundance and '-' sign refers to absence)

Among these SMs derived from the SILE, the flavonoids should have the most efficient compounds to enhance the high corrosion inhibiting actions because it reported that the leaf extract of this plant had high amounts (about 66 mg/g) of flavone in the literature (Liu *et al*., 2022). These findings align with existing literature (Dossou *et al*., 2021). The secondary metabolites (SMs) from SILE contribute to forming a diffusion-barrier passive layer on the surface of 500MS rebar through the adsorption phenomenon, which aids in controlling corrosion and is consistent with previous studies (Hussain, 2014).

UV-visible spectra are useful for identifying compounds that contain aromatic rings, chromophores, lone pairs of electrons, σ-bonds, and π-bonds. The UV-Vis spectra of SILE exhibit peaks at 409 nm, 471 nm, 532 nm, 603 nm, 664 nm, and 742 nm, as illustrated in Fig. 2(a), indicating the presence of aromatic or conjugated unsaturated systems (Sudhashini *et al*., 2023). Furthermore, Fig. 2(b) presents the results of the functional groups identified in the secondary metabolites (SMs) of SILE by FTIR spectra. A peak at 3350 cm^{-1} is associated with O-H or N-H stretching vibrations in aromatic compounds (Sulistiawan *et al*., 2022). The SILE demonstrates a peak approximately at 2920 cm^{-1}, which signifies asymmetric stretching of C-H vibrations. Furthermore, the presence of peaks within the range of 1600 to 1730 cm^{-1} suggests the existence of carbonyl (C=O) and C=C functional groups in aromatic compounds (Yue *et al*., 2018). These findings collectively confirm the presence of various functional groups, including alcohols, amines, ketones, acids, and unsaturated compounds. Besides, a peak observed at 1020 cm^{-1} corresponds to O-H or C=N bending vibrations in aromatic compounds (Saifitri *et al*., 2021). These FTIR analysis confirmed the existence of heteroatoms such as nitrogen (N) and oxygen (O), along with functional groups including phenols, aromatics, carboxylic acids, and amines, which were made distinctive by their richness in unsaturation (Sukhikh *et al*., 2022).

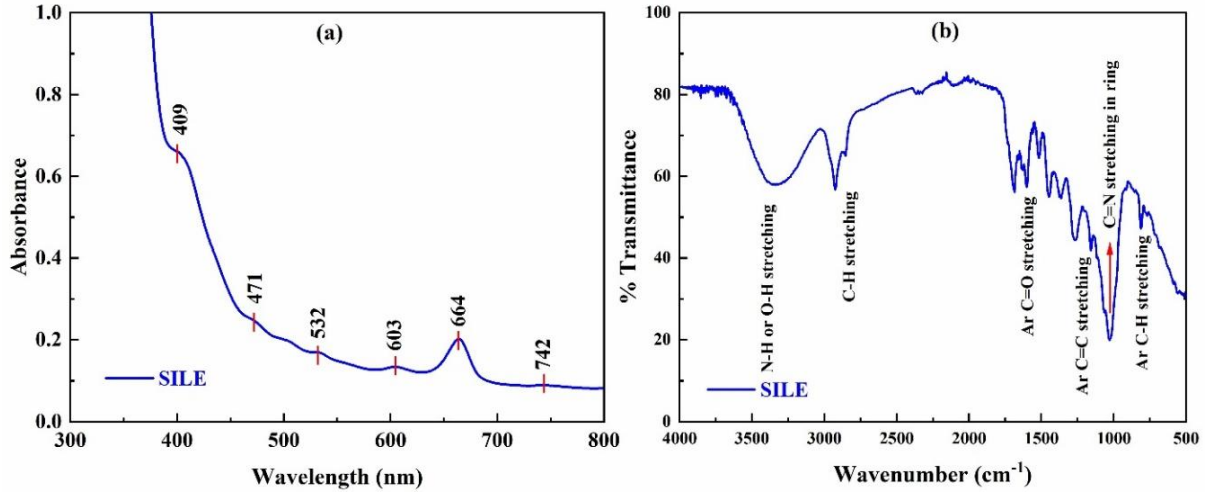

Figure 2. UV-Vis (a) and FT-IR (b) spectra of SILE.

More than nine SMs, mostly the flavonoids, including alkaloids, terpenoids, and others, are identified by ultra high performance liquid chromatography (UHPLC) analysis of the SILE in this study employing mass bank matching, as tabulated in Table 2 and as illustrated in Fig. 3. The literature also supports this, reporting that fresh leaves of the *S. indica* L. plant had the highest flavone of 65.7 mg/g than other SMs (Liu *et al*., 2022). These SMs of SILE establish the truth by phytochemical, UV-Vis, and FTIR tests in the present works.

Table 2. Major compounds present in SILE analyzed from UHPLC.

S. N.	Retention time (min.)	Molecular formula & weight (g/mol)	Name of compounds	Compound types
1	0.720	$C_{14}H_{19}NO_2$ (233.1)	Metolachlor morpholinone	Alkaloid
2	5.151	$C_{21}H_{18}O_{13}$ (478.1)	Quercetin-3-O-glucoside	Flavonoid
3	5.507	$C_{15}H_{14}O_6$ (290.3)	D-(+)-Catechin	Polyphenol
4	6.132	$C_{20}H_{21}NO_4$ (339.1)	Canadine or Papaverine	Alkaloid
5	6.775	$C_{15}H_{12}O_3$ (240.1)	4'-Hydroxyflavone	Flavonoid
6	8.602	$C_{27}H_{28}O_{16}$ (596.2)	Eriodictyol-7-neoherperidoside	Flavonoid
7	10.868	$C_{29}H_{30}O_{17}$ (650.1)	Genistein xylosylglucoside malonylated	Flavonoid
8	11.122	$C_{15}H_{11}O_6^+$ (287.2)	Cyanidin	Flavonoid
9	11.528	$C_{28}H_{38}O_{17}$ (646.2)	Haploperozide	Terpenoid

These investigations showed that SILE has a strong anti-corrosive effect on concrete reinforcement corrosion due to the presence of substances such as canadine, quercettin-3-o-glucoside, D-(+)-catechin, 4'-hydroxyflavone, cyanidin, and others. It is made possible by the compounds contained in SILE adhering to the 500MS specimens dipped in simulated CPS either chemically through ionic or co-covalent bonding or physically through Van der Waals interactions (Rajendran *et al.*, 2024).

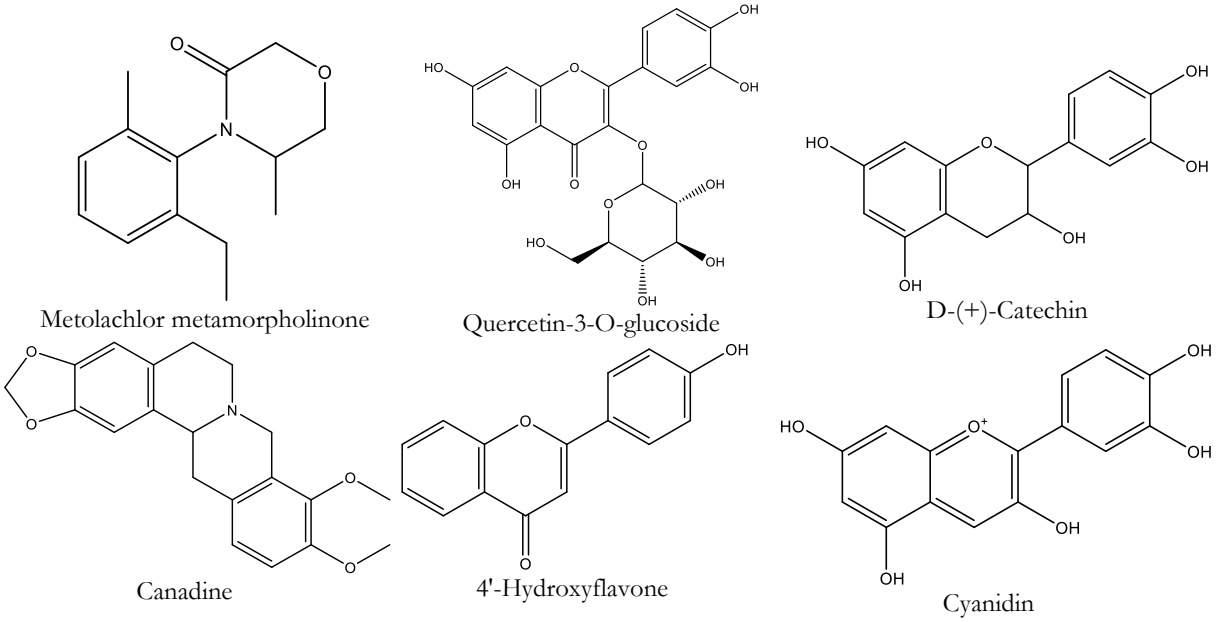

Figure 3. The molecular structure of some secondary metabolites is present in SILE by UHPLC analysis.

The strong anti-corrosive effect or corrosion inhibitory action of these SMs extracted from the leaves of *the Sesamum indica* L. plant on the 500MS in simulated CPS is studied using two methods: weight loss and electrochemical polarization analysis. Initially, the weight loss (WL) approach was employed to determine the corrosion rate (CorR) and corrosion inhibition efficiency (CorIE), followed by a potentiodynamic polarization (PDP) analysis. As illustrated in Fig. 4(a), the CorR of 500MS specimens immersed in CPS containing 500–4000 ppm of SILE decreased over time compared to the control CPS (which did not contain SILE). Furthermore, as the concentration of SILE in CPS increased, the CorR of the 500MS specimens further decreased, demonstrating an enhanced corrosion inhibition effect. It is meaningful to mention that as shown in Fig. 4(a), the corrosion rate is increased very slightly after about 1500 hrs exposure, especially in 500 and 1000 ppm SILE additions, and such effect is less seen at high concentrations between 2000-4000 ppm SILE. However, the corrosion inhibition efficiency at high concentrations, 2000-4000 ppm, attains a steady state. It means a stable and anti-corrosive passive film formed at high concentrations, compared with low concentrations of SILE. It became evident that the corrosion inhibition for the immersed 500MS specimens improved with rising SILE concentrations.

The highest corrosion inhibition efficiency (CorIE) was observed after 2134 hours of immersion in CPS with 4000 ppm SILE, reaching approximately 96%, as shown in Fig. 4(b). According to qualitative chemical testing, spectroscopic, and chromatographic examinations as described above, the SILE contains a variety of flavonoids, alkaloids, phenolics, and terpenoids. These SMs act as focal regions for molecular interactions with

the corroded surfaces of 500MS specimens in the simulated CPS because SMs are composed of heteroatoms and conjugated aromatic π-electrons (Wang *et al.*, 2023).

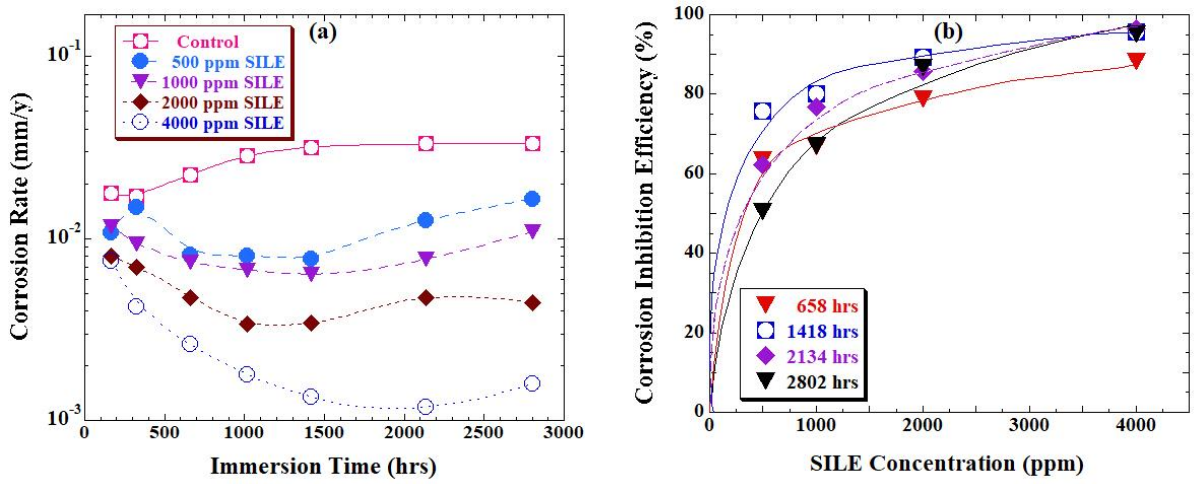

Figure 4. Variation of (a) corrosion rate of 500MS specimens immersed in CPS without and with SILE and (b) corrosion inhibition efficiency at different immersion times in CPS with 500-4000 ppm SILE.

Langmuir and Temkin isotherms are essential for explaining the molecular interactions between SMs of SILE and corroded mild steel specimens. Figure 5(a) shows the Langmuir adsorption isotherms between C/θ and C of SILE after different immersion times with 500-4000 ppm concentrations. Coefficient of determination (R^2) and slop of the straight line is nearly unit. The isotherms evaluated the inhibitory mechanism of SILE onto corroded 500MS specimens in CPS with SILE concentration.

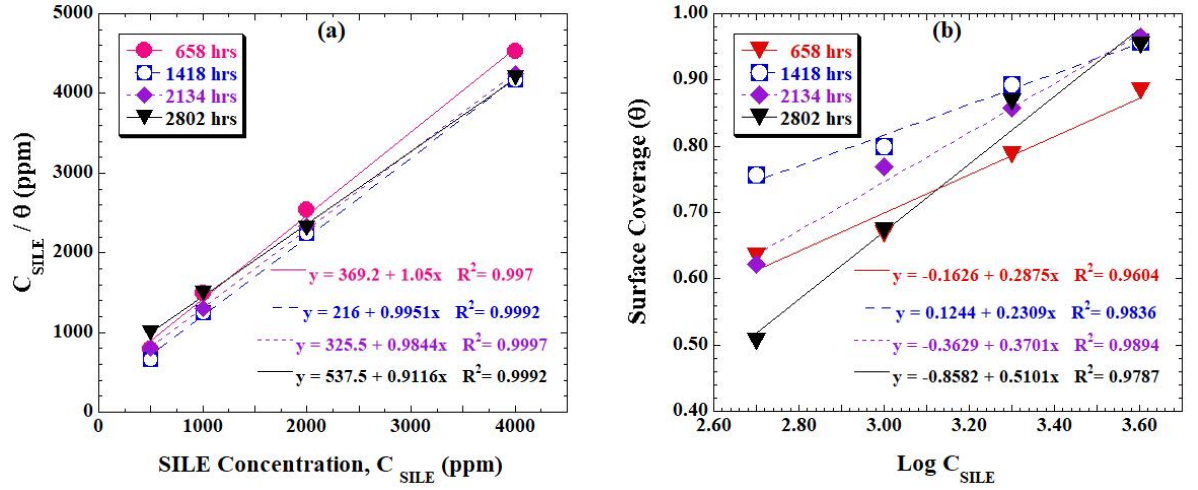

Figure 5. (a) Langmuir isotherm plots and (b) Temkin isotherm plots for 500MS specimens in CPS with different concentrations of SILE at different immersion times.

Therefore, this isotherm refers to the monolayer adsorption of SMs onto the corroded 500MS specimens in CPS with varying concentrations of SILE. Similarly, in Temkin isotherm, a linear relationship between θ and Log C of SILE after varying immersion times was obtained. However, R^2 values range from 0.960 to 0.989, which are comparatively less than those in Langmuir isotherm (Fig. 5b), indicating uniform monolayer adsorption of SILE's SMs onto the corroded 500MS specimens in CPS, as described elsewhere (Adejo *et al.*, 2024). Thus, Langmuir adsorption isotherm is the best fit than Temkin adsorption isotherm. These results are aligned with outcomes of previous literature that documented similar adsorption behavior of plant-derived phyto-compounds (i.e., SMs) on the corroded mild steel in acidic solutions (Bhardwaj *et al.*, 2021).

In addition to the weight loss (WL) technique, the corrosion inhibition kinetic of SILE was investigated on the 500MS surface in CPS without and with SILE using PDP analysis. The corrosion potential (ϕ_{cor}) values moved in more negative (cathodic) directions with varying SILE concentrations. The ϕ_{cor} of the sample in control CPS is -428 mV (SCE), which is shifted to -560, -525, -505, and -530 mV (SCE) in CPS with 500, 1000, 2000, and 4000 ppm SILE, as shown in Figs. 6(a), 6(b),

6(c), and 6(d), respectively, and summarized in Table 3. The results of the shifting of ϕ_{cor} with SILE concentrations in CPS do not show regular trends. However, the shifting of ϕ_{cor} is more than -77 mV, and it does not show a significant change of anodic current density with changing the SILE concentration, suggesting SILE is a cathodic type of corrosion inhibition by reducing oxygen or hydrogen reduction reactions (Nam *et al.*, 2018). Besides, SILE concentration increases in CPS, the corrosion current density (i_{cor}) of the polarized 500MS sample specimen decreases with increasing the SILE concentrations in CPS, as summarized in Table 3, indicating that the SILE inhibitor creates a protective layer that stops further dissolution of 500MS. In contrast, a higher i_{cor} in control CPS without SILE extract indicates a higher corrosion rate, meaning the 500MS is corroding quickly (Abouchane *et al.*, 2022).

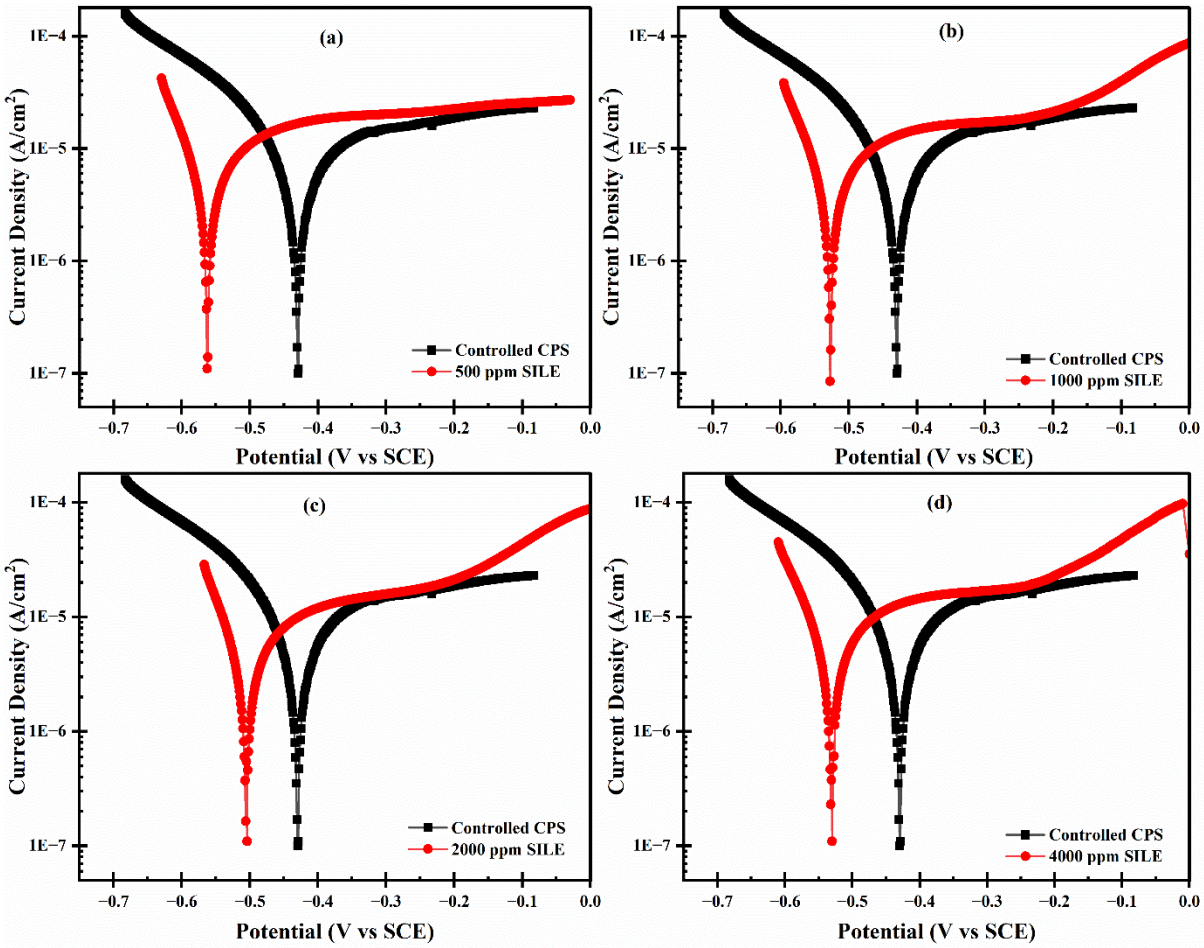

Figure 6. Polarization curves for 500MS specimens immersed in CPS with (a) 500 ppm, (b) 1000 ppm, (c) 2000 ppm, and (d) 4000 ppm of SILE compared with controlled CPS (without SILE).

Corrosion rate and inhibition efficiency were also calculated from ϕ_{cor}, i_{cor}, Tafel's slope of the anode (β_a) and cathode (β_c) from PDP curves, as illustrated in Fig. 6. These kinetic parameters sum up in Table 3 according to the Tafel extrapolation method. Changes in the electrochemical kinetics of corrosion, frequently brought on by SILE in CPS, are shown by an increase in the anodic (β_a) and cathodic (β_c) slopes of Tafel curves. It implies that polarization resistance (R_p) encourages improvement through limited anodic metal dissolution and cathodic reduction (such as oxygen or hydrogen reduction) processes. Increased β_c implies impeded reduction reactions because of surface obstruction or diffusion limits, whereas higher β_a indicates slower metal dissolution and potential surface passivation (Amin *et al.*, 2014). The development of a passive layer, enhanced R_p, and decreased overall corrosion rates are ultimately indicated by this trend (Loto, 2018).

In literature, estimations based on corrosion current density and weight loss measurements showed that the CorIE of 4000 ppm leaf extract of *Tagetes erecta* is 73.78% and 67.81%, respectively (Gautam *et al.*, 2024b). In addition, the CorIE of 4000 ppm leaf extract from *Ziziphus budhensis* exhibited 81.48% based on i_{corr} and 91.22% based on WL (Gautam *et al.*, 2024a). However, in present studies, 4000 ppm leaf extract of *Sesamum indicum* (SILE) demonstrated inhibition efficiencies of 81.7% (i_{corr}-based) and 93.9% (WL-based). These findings from previous studies indicated that SILE is a more effective corrosion inhibitor for reinforced concrete than other plant-based leaf extracts.

Table 3. Polarization and weight loss parameters determined from linear polarization resistant (LPR) method and weight loss after 2802 hrs of immersion in CPS.

SILE amount (ppm)	ϕ_{cor} (mV)	i_{cor} ($\mu A/cm^2$)	β_a (mV/dec	β_c (mV/dec)	R_p ($K\Omega.cm^2$)	i_{cor}-based CorR (mpy)	i_{corr}-based CorIE (%)	WL-based CorR (mpy)	WL-based CorIE (%)
000	-428	7.301	2.54	6.33	0.04	6.75	-	0.03399	-
500	-560	3.712	7.94	15.41	1.77	3.43	49.2	0.01410	58.5
1000	-525	2.477	13.34	18.43	7.27	2.29	66.1	0.00855	74.8
2000	-505	1.654	19.21	21.97	24.19	1.53	77.4	0.00582	82.9
4000	-530	1.339	27.02	32.36	89.29	1.24	81.7	0.00209	93.9

After immersing 500MS specimens in simulated CPS for 2802 hours, both without and with 4000 ppm of SILE, we examined how the morphological surfaces of the specimens had changed. Figure 7(a) illustrates that the specimen immersed in CPS without SILE exhibited a heavily corroded surface with corrosion-related defects (May, 2016). Prolonged submersion in the control CPS resulted in significant corrosion, as the surface defects facilitated the interaction of aggressive ions with the metal surface. In contrast, Fig. 7(b) presents SEM micrographs of specimens after immersion in CPS containing 4000 ppm of SILE for the same duration. These specimens displayed smooth surfaces with very few corrosion-related defects and minimal corrosion products, highlighting the substantial anti-corrosive effectiveness of SILE in CPS. When aggressive ions penetrate, the protective adsorption layer serves as a shield (Muthukrishnan *et al.*, 2015).

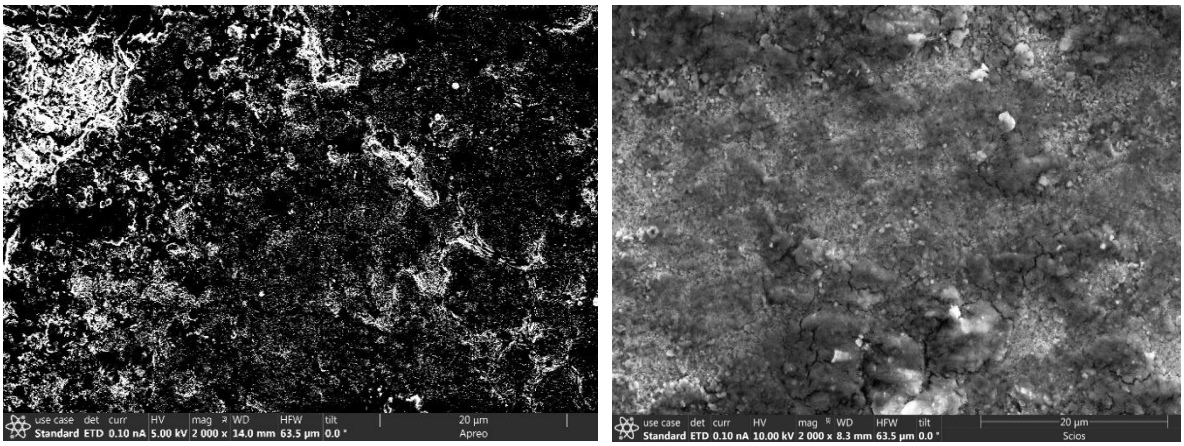

(a) **(b)**

Figure 7. SEM micrograph for the adsorption layer formed over MS specimens after immersing it for 2802 hours in (a) control CPS & (b) CPS with 4000 ppm SILE.

Alongside the SEM analysis, we observed that the iron content of the 500MS specimens decreased significantly, dropping from 98.37% to 55.43%. This reduction was accompanied by a notable increase in oxygen levels, reaching 29.38%, as determined by elemental analysis using EDS. This change indicates the formation of corrosion products in the sample exposed to the control CPS without SILE. In contrast, the specimens immersed in CPS containing 4000 ppm of SILE for 2802 hours exhibited fewer corrosion products on the surface of the immersed 500MS specimen. The iron and oxygen levels for the sample are 70.09% and 22.69%, respectively, as summarized in Table 4. Consistent with previous studies (Verma & Khan, 2016), the surface morphology of the 500MS immersed in CPS with SILE showed significantly less corrosion, indicated by a notably low quantity of rust. It is also attributable to higher iron and lower oxygen content in the specimen. Hence, SILE reduces the iron dissolution in CPS and acts as an anti-corrosive agent.

Table 4. Elemental analysis of 500MS specimens in control CPS and CPS with 4000 ppm SILE after 2802 hours of immersion

Medium	Composition (wt.%)				
	Fe	**O**	**C**	**Si**	**Misc.**
Fresh 500MS specimen	98.37	–	00.17	00.40	01.08
500MS after immersion for 2802 hrs. in control CPS	55.43	29.38	11.37	02.12	01.70
500MS after immersion for 2802 hrs. in CPS with 4000 ppm SILE	70.09	22.69	–	02.05	05.17

The WLI technique, a very sensitive tool for corrosion investigations, was used to examine surface roughness and surface morphology (Lei *et al.*, 2019). These approaches also offer non-destructive, quick, precise, and non-contact three-dimensional topographic profiling of corroded metal with lateral and vertical resolution (Tao *et al.*, 2019). The 2D and 3D surface profiles of the 500MS specimen after 2802 hours of immersion in CPS containing 4000 ppm of SILE are shown in Figs. 8(a) and 8(b), respectively. The surface roughness value for this specimen is 6.607 µm, as illustrated in Fig. 8(a). This value is lower than the surface roughness value of 8.510 µm, which was reported for the WLI images of the 500MS specimen exposed to 2802 hours in control CPS without plant extract in the literature (Gautam *et al.*, 2024a). The result showed that the surface roughness of 500MS specimens dipped in CPS with 4000 ppm of SILE decreased by 22.36% compared with control CPS. These findings align with the findings of SEM analysis. As a result, SILE performs better in corrosion inhibition of mild steel specimens.

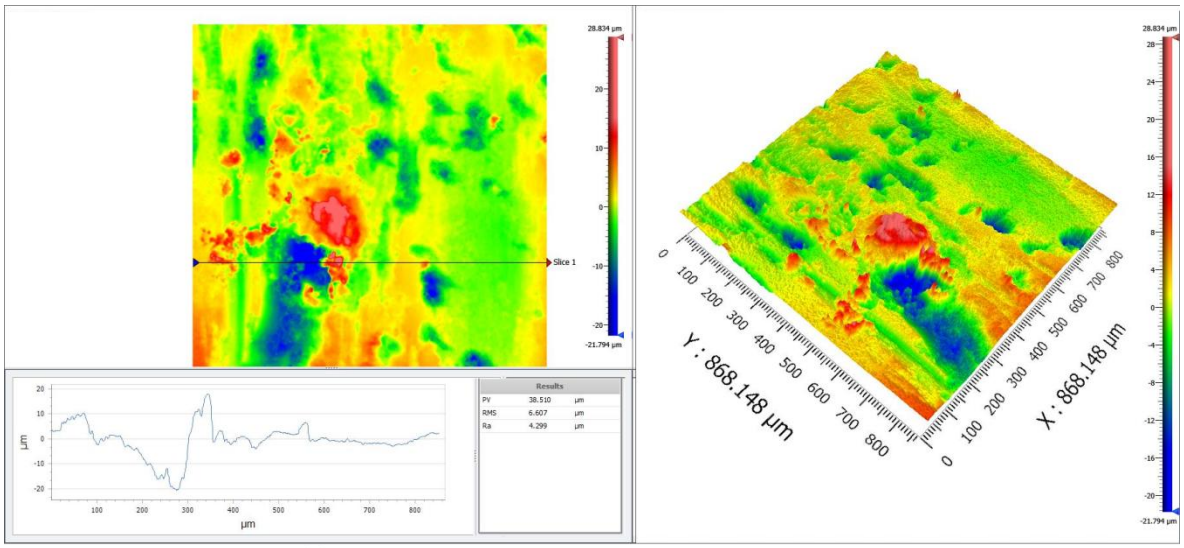

Figure 8. 2D (a) and 3D (b) WLI images of the 500MS specimens after 2802 hrs of immersion in CPS with 4000 ppm SILE.

The above discussion of the results from corrosion tests, inhibition efficiency, adsorption, and electrochemical analyses suggested that SILE exhibits superior corrosion-inhibiting characteristics in simulated CPS or the reinforcement concrete environment. The result aligns with the corrosion morphology analysis conducted through SEM/EDS and WLI techniques. A graphical representation elucidates the corrosion-inhibiting mechanism of mild steel corrosion control by adsorption of plant-based SMs of SILE in simulated CPS without (control) and with 500-4000 ppm SILE in ambient conditions to clarify such noble inhibiting action of SILE in CPS (Fig. 9).

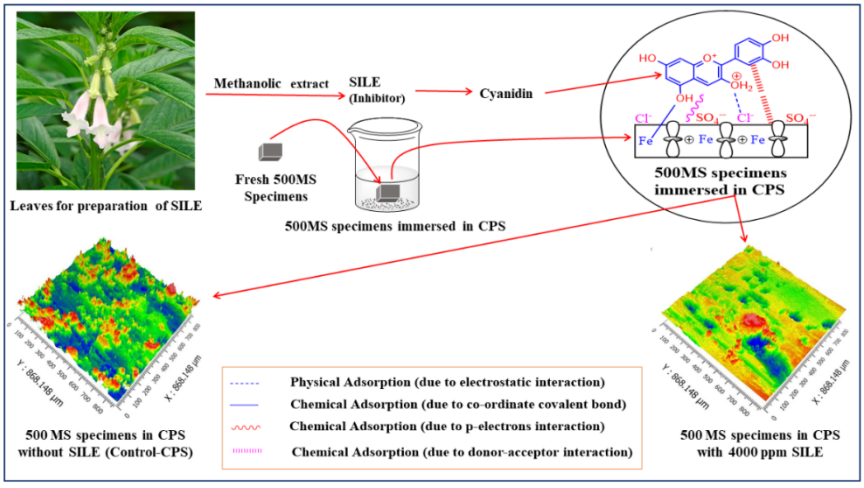

Figure 9. Diagrammatic representation of how the adsorption of the cyanidin molecule, one of the phytochemicals of SILE, inhibits corrosion of MS specimen without SILE (control-CPS) and with 4000 ppm SILE in the CPS at ambient condition.

According to the corrosion inhibition mechanism of SMs of SILE to the corroded mild steel (MS) either in CPS or reinforcement concretes, four interactions are involved in the adsorption of the passive layer formed onto the MS specimen immersed in CPS with plant-based SMs (for example the cyaniding), as illustrated in Fig. 9. In this model of the corrosion control of MS by SMs constituents of SILE either in simulated CPS or ReC follows the steps below.

* Heteroatoms found in SILE constituents (such as flavonoids, polyphenols, alkaloids, and terpenoids) undergo physical adsorption through electrostatic interactions to protonate and stick SMs of SILE to the positively charged surface of the corroded MS specimens or Fe^{2+} ions (Zakeri *et al.*, 2022).
* Chemical adsorption might occur via coordination bonding between lone pairs (non-bonding electrons) on atoms such as O or N in SMs and the vacant d-orbitals of Fe-atoms in the MS specimens (Wei *et al.*, 2022).
* Chemical adsorption is promoted by π-electrons interactions between the aromatic ring and the vacant d-orbitals of Fe-atoms in the MSR (Verma *et al.*, 2024).
* Chemical adsorption due to retro-donation or donor-acceptor interactions between d-electrons of Fe-atoms of the corroded mild steel and empty anti-bonding molecular orbitals of SMs constituents of SILE (Ebenso *et al.*, 2010).

Therefore, the SMs derived from SILE are sufficient to create an anti-corrosive passive adsorption film on the surface of the corroded MS specimen due to numerous adsorption sites, and they act as efficient corrosion inhibitors. This study investigates the SMs, isolated from native *Sesamum indicum* leaves, as environmentally acceptable plant-based inhibitors either in CPS or reinforcement concretes as admixtures for the first time in controlling the corrosion of MS in CPS.

CONCLUSIONS

This study demonstrates that first-time use of SILE effectively prevents the corrosion of 500MS specimens in simulated concrete pore solution (CPS). Results from weight loss (WL), potentiodynamic polarization (PDP), and surface analysis like SEM/EDS, WLI confirm the formation of a protective surface layer that slows down the corrosion rate of 500MS in CPS containing 500-4000 ppm SILE as a concrete admixture. The optimal inhibition efficiencies achieved were 93.9% (measured by WL) and 81.7% (measured by PDP) at 4000 ppm SILE in simulated CPS at room temperature. The PDP measurements indicate that the cathodic reaction primarily governs the effectiveness of SILE as a significant corrosion inhibitor.

The Langmuir and Temkin adsorption isotherms suggest that the SILE-based secondary metabolites (SMs) create a homogeneous, single-layer protective coating on the surface of the corroded 500MS through physical adsorption. Compared to the 500MS sample immersed in control CPS without SILE, surface characterization using 2D-SEM/EDS and 3D-WLI revealed that the surface of the 500MS remained smooth after immersion for about four months or more in CPS with SILE. This study encourages researchers to explore the anti-corrosive properties of new plant-based extracts in the future for potential use such as waterproofing or corrosion-resistant concrete admixtures.

ACKNOWLEDGEMENTS

The authors thank the University of Cincinnati (Dr. M.A. Fickenscher) for SEM/EDS facilities and IMR-CAS in Shenyang, China, for WLI support. MG appreciates the University Grant Commission (UGC-Nepal) for funding his Ph.D. research grants (Award No.: PhD-78/79-S&T-03).

AUTHOR CONTRIBUTION STATEMENT

MG, NPB & JB designed experiments; sample preparation, experimental works, and data analysis by MG; examined the data and results summarization by MG, NPB, and JB; wrote the manuscript draft by MG and NPB and did the final corrections by JB. All authors read and approved of the final manuscript.

CONFLICT OF INTEREST

The authors claim that they have no competing interests.

DATA AVAILABILITY STATEMENT

Upon reasonable request, the corresponding authors will provide the data supporting the study's conclusions.

REFERENCES

Abdel-Karim, A.M., & El-Shamy, A.M. (2022). A review on green corrosion inhibitors for protection of archeological metal artifacts. *Journal of Bio- and Tribo-Corrosion*, *8*, 35. http://dx.doi.org/10.1007/s40735-022-00636-6.

Abouchane, M., Dkhireche, N., Rbaa, M., Benhiba, F., Ouakki, M., Galai, M., Lakhrissi, B., Zarrouk, A., & Touhami, M.E. (2022). Insight into the corrosion inhibition performance of two quinoline-3-carboxylate derivatives as highly efficient inhibitors for mild steel in acidic medium: experimental and theoretical evaluations. *Journal of Molecular Liquids*, *360*, 119470. https://doi.org/10.1016/j.molliq.2022.119470.

Adejo, S., Uzah, T.T., & Akuhwa, J. (2024). Adsorption isotherm modeling in corrosion inhibition studies. In book: *Corrosion Engineering - Recent Breakthroughs and Innovative Solutions*, 1-15. http://dx.doi.org/10.5772/intechopen.1005211.

Amagain, K., Subedi, B.N., Joshi, S., & Bhattarai, J. (2022). A comparative study of the anticorrosive response of *Tinospora cordifolia* stem extract for Al and

Cu in biodiesel-based fuels. *E3S Web of Conferences*, *355***,** 01005. https://doi.org/10.1051/e3sconf/202235501005.

Amin, M., El-Bagoury, N., Saracoglu, M., & Ramadan, M. (2014). Electrochemical and corrosion behavior of cast re-containing Inconel 718 alloys in sulphuric acid solutions and the effect of Cl^-. *International Journal of Electrochemical Science, 9*(9), 5352-5374. http://dx.doi.org/10.1016/S1452-3981(23)08171-3.

Bhardwaj, N., Sharma, P., & Kumar, V. (2021). Phytochemicals as steel corrosion inhibitor: an insight into mechanism. *Corrosion Reviews*, *39*(1), 27-41. http://dx.doi.org/10.1515/corrrev-2020-0046.

Bhattarai, J. (2010). *Frontiers of corrosion science* (1st ed.), Kshitiz Publication, Kirtipur, Nepal, p. 304.

Bhattarai, J., Somai, M., Acharya, N., Giri, A., Roka, A., & Phulara, N. (2021). Study on the effects of green-based plant extracts and water-proofers as anti-corrosion agents for steel-reinforced concrete slabs. *E3S Web of Conferences*, *302*(1), 02018. http://dx.doi.org/10.1051/e3sconf/202130202018.

Deyab, M.A., & Mohsen, Q. (2023). Inhibitory capabilities of sweet yellow capsicum extract toward the rusting of steel rebars in cement pore solution. *ACS Omega*, *8*(3), 3303-3309. http://dx.doi.org/10.1021/acsomega.2c06639.

Dossou, S.S.K., Xu, F., Cui, X., Sheng, C., Zhou, R., You, J., Tozo, K, & Wang, L. (2021). Comparative metabolomics analysis of different sesame (*Sesamum indicum* L.) tissues reveals a tissue-specific accumulation of metabolites. *BMC Plant Biol*ogy, *21*, 352 (2021). https://doi.org/10.1186/s12870-021-03132-0.

Fuhaid, A.F.A., & Niaz, A. (2022). Carbonation and corrosion problems in reinforced concrete structures. *Buildings, 12*(5), 586. https://doi.org/10.3390/buildings12050586.

Fuji, Y., Uchida, A., Fukahori, K., Chino, M., Ohtsuki, T., & Matsufuji, H. (2018). Chemical characterization and biological activity in young sesame leaves (*Sesamum indicum* L.) and changes in iridoid and polyphenol content at different growth stages. *PLoS ONE, 13*(3), e0194449. https://doi.org/10.1371/journal.pone.0194449.

Gagg, C.R. (2014). Cement and concrete as an engineering material: an historic appraisal and case study analysis. *Engineering Failure Analysis*, 40. http://dx.doi.org/10.1016/j.engfailanal.2014.02.004.

Gautam, M., Bhattarai, N.P., & Bhattarai, J. (2024a). Gravimetric and electrochemical interpretation of plant extract as corrosion inhibitor for embedded-steel in concrete pore solution. In *proceedings of 10th International Conference on CONcrete under SEvere Conditions – Environment and Loading 2024*, Chennai, India, pp. 784-792.

Gautam, M., Bhattarai, N.P., & Bhattarai, J. (2024b). Leaf-based extracts of Nepal origin plants as efficient inhibitors for controlling rebar corrosion in concrete pore solution. *International Journal of Corrosion and Scale Inhibition*, *13*(4), 2087-2111. http://dx.doi.org/10.17675/2305-6894-2024-13-4-10.

Gautam, M., Subedi, D.B., Dhungana, J.R., Bhattarai, N.P., & Bhattarai, J. (2025). Utilization of bark extract of *Phyllanthus emblica* as a sustainable corrosion inhibitor to reinforced concrete infrastructures in aggressive environments. *E3S Web of Conferences*, *610*, 03002. https://doi.org/10.1051/e3sconf/202561003002.

Giri, A., Gautam, M., Roka, A., Bhattarai, N.P., & Bhattarai, J. (2023). Performance of anticorrosive measures of steel in concrete infrastructures by plant-based extracts. *Macromolecular Symposia*, *410*(1), 2200115. https://doi.org/10.1002/masy.202200115.

Harb, M.B., Abubshait, S., Etteyeb, N., Kamoun, M., & Dhouib, A. (2020). Olive leaf extract as a green corrosion inhibitor of reinforced concrete contaminated with seawater. *Arabian Journal of Chemistry*, *13*(3), 4846-4856. http://dx.doi.org/10.1016/j.arabjc.2020.01.016.

Hau, N.N., & Huong, D.Q. (2022). Effect of aromatic rings on mild steel corrosion inhibition ability of nitrogen heteroatom-containing compounds: experimental and theoretical investigation. *Journal of Molecular Structure*, *1277*(2), 134884. http://dx.doi.org/10.1016/j.molstruc.2022.134884.

Hussain, R.R. (2014). Passive layer development and corrosion of steel in concrete at the nano-scale. *Journal of Civil & Environmental Engineering*, *04*(03), 1-4. http://dx.doi.org/10.4172/2165-784X.1000e116.

Jabed, A., Tusher, M.M.H., Shuvo, Md.S.I., & Imam, A. (2023). Corrosion of steel rebar in concrete: a review. *Corrosion Science and Technology*, *22*(4), 272-286. https://doi.org/10.14773/cst.2023.22.4.273.

Jagadesh, P., Juan-Valdés, A., Guerra-Romero, M.I., Morán-del Pozo, J.M., García-González, J., & Martínez-García, R. (2021). Effect of design parameters on compressive and split tensile strength of self-compacting concrete with recycled aggregate: an overview. *Applied Sciences*, *11*(13), 6028. https://doi.org/10.3390/app11136028.

Keles, B., Bakhytzhan, A., Karashina, A., & Nurakhova, A. (2023). Identifying the influence of expanded clay concrete based on a binder from phosphorus slag on the strength of structures from leaked concrete. *Eastern-European Journal of Enterprise Technologies*, *4*(6), 51-58. http://dx.doi.org/10.15587/1729-4061.2023.285183.

Langmuir, I. (1916). The constitution and fundamental properties of solids and liquids: Part I-solid. *Journal of the American Chemical Society*, *38(*11), 2221-2295. https://doi.org/10.1021/ja02268a002.

Lei, Z., Liu, X., Zhao, L., Yang, W., Chen, C., & Xiaoting, G. (2019). A rapid measurement method for structured surface in white light interferometry. *Journal of Microscopy*, *276*(3), 118-127. http://dx.doi.org/10.1111/jmi.12843.

Liu, H., Zhou, F., Zhou, T., Yang, Y., & Zhao, Y. (2022). A novel wrinkled-leaf sesame mutant as a potential edible leafy vegetable rich in nutrients. *Scientific Report*, *12*, 18478. https://doi.org/10.1038/s41598-022-23263-0.

Loto, R.T. (2018). Electrochemical analysis of the corrosion inhibition effect of trypsin complex on the

pitting corrosion of 420 martensitic stainless steel in 2M H_2SO_4 solution. *Plos One*, *13*(4), e0195870. https://doi.org/10.1371/journal.pone.0195870

Maeda, M., Li, X., Ooi, A., Tada, E., & Nishikata, N. (2020). Passivation mechanism of galvanized steel rebar in fresh concrete, *ISIJ International*, 60(2), 337–345. https://doi.org/10.2355/isijinternational.ISIJINT-2019-396.

Magrati, P., Subedi, D.B., Pokharel, D.B., & Bhattarai, J. (2020). Appraisal of different inorganic inhibitors action on the corrosion control mechanism of mild steel in HNO_3 solution. *Journal of Nepal Chemical Society*, *41*(1), 64-73. https://doi.org/10.3126/jncs.v41i1.30489.

May, M. (2016). Corrosion behavior of mild steel immersed in different concentrations of NaCl solutions. *Journal of Sebha University (Pure and Applied Sciences)*, *15*, 1-12. https://repository.sebhau.edu.ly/handle/1/57.

Mukta, N., & Neeta, M.P. (2017). A review on sesame-an ethno-medicinally significant oil crop. *International Journal of Life Sciences and Pharmaceutical Research, 7*(2), 58-63.

Muthukrishnan, P., Prakash, P., Jeyaprabha, B., & Shankar, K. (2015). Stigmasterol extracted from *Ficus hispida* leaves as a green inhibitor for the mild steel corrosion in 1M HCl solution. *Arabian Journal of Chemistry*, 12(8), 3335-3356. http://dx.doi.org/10.1016/j.arabjc.2015.09.005.

Nagendra, P.M.N., Sanjay, K.R., Prasad, D.S., Vijay, N., Kothari, R., & Nanjunda, S. (2012). A review on nutritional and nutraceutical properties of sesame. *Journal of Nutrition & Food Sciences, 2*(1), 1-6. http://dx.doi.org/10.4172/2155-9600.1000127.

Nam, N.D., Hien, P.V., Hoai, N.T., & Thu, V.T.H. (2018). A study on the mixed corrosion inhibitor with a dominant cathodic inhibitor for mild steel in aqueous chloride solution. *Journal of the Taiwan Institute of Chemical Engineers*, *91*, 556-569. http://dx.doi.org/10.1016/j.jtice.2018.06.007.

Narasimhan, R., & Mohan, A. (2012). Phytochemical screening of *Sesamum indicum* seed extract. *World Journal of Pharmacy and Pharmaceutical Sciences, 1,* 1298–1308.

Oyekunle, D.T., Oguntade, T.I., Ita, C.S., Ojo, T., & Orodu, O.D. (2019). Corrosion inhibition of mild steel using binary mixture of sesame and castor oil in brine solution. *Materials Today Communications, 21*, 100691. https://doi.org/10.1016/j.mtcomm.2019.100691.

Popoola, P., Abdulwahab, M., & Fayomi, O.S.I. (2012). Corrosion inhibition of mild steel in *Sesamum indicum*-2M HCl/H_2SO_4 interface. *International Journal of Electrochemical Science, 7*, 5805–5816. https://doi.org/10.1016/S1452-3981(23)19444-2.

Rajendran, S., Al-Hashem, A., Krishnaveni, A., Arockiaraj, L.J., Singh, G., Lacnjevac, C., Jothi, M.N., & Shanthy, P. (2024). Corrosion inhibition by fruit extracts-inhibition of corrosion of mild steel in simulated concrete pore solution prepared in sea water by an aqueous extract of apple juice- a case study. *Zastita Materijala*, *65*(2024), 22-34. https://doi.org/10.62638/ZasMat1040.

Rana, M., Joshi, S., & Bhattarai, J. (2017). Extract of different plants of nepalese origin as green corrosion inhibitor for mild steel in 0.5 m NaCl solution. *Asian Journal of Chemistry*, *29*(5), 1130-1134. https://doi.org/10.14233/ajchem.2017.20449.

Saifitri, E., Humaira, H., Nazaruddin, N., Susilawati, S., Murniana, M. & Md Sani, N.D. (2021). *Dioscorea Alata* L. anthocyanin extract as methanol as a sensitive pH active compound. *Journal of Physics Conference Series*, *1869*(1), 012508. http://dx.doi.org/10.1088/1742-6596/1869/1/012058.

Somai, M., Giri, A., Roka, A., & Bhattarai, J. (2023). Comparative studies on the anti-corrosive action of waterproofing agent and plant extract to steel rebar. *Macromolecular Symposia*, *410*(1), 2100276. https://doi.org/10.1002/masy.202100276.

Subedi, B.N., Amgain, K., Joshi, S., & Bhattarai, J. (2019). Green approach to corrosion inhibition effect of *Vitex negundo* leaf extract on aluminum and copper metals in biodiesel and its blend. *International Journal of Corrosion and Scale Inhibition*, *8*(3), 744−759. https://doi.org/10.17675/2305-6894-2019-8-3-21.

Sudhashini, S., Amudha, P., Vidhya, R., Rani, V., & Satheesh, R.K. (2023). Phytochemical screening and profiling of secondary metabolites of *Annona muricata* bark. *Journal of Advance Zoology*, *44*(4), 329-339. http://dx.doi.org/10.17762/jaz.v44i4.1685.

Sukhikh, S., Prosekov, A., Ivanova, S., Maslennikov, P., Andreeva, A., Budenkova, E., Kashirskikh, E., Tcibulnikova, A., Zemliakova, E., Samusev, I., & Babich, O. (2022). Identification of metabolites with antibacterial activities by analyzing the FTIR spectra of microalgae. *Life*, *12*(9), 1395. https://doi.org/10.3390/life12091395.

Sulistiawan, A., Setyaningsih, W., & Rohman, A. (2022). A new FTIR method combined with multivariate data analysis for determining aflatoxins in peanuts (*Arachis hypogaea*). *Journal of Applied Pharmaceutical Sciences*, *12*(7), 199-206. http://dx.doi.org/10.7324/JAPS.2022.120720.

Tao, C.K., Wu, Y.J., Wang, W.Y., Qian, Y.S., Tao, R., & Kang, T. (2019). Experimental investigation of white-light interferometry based on sub-dark-field illumination. *Optics Communications*, *435*, 108-117. https://doi.org/10.1016/j.optcom.2018.11.020.

Temkin, M.I. (1941). Adsorption equilibrium and the kinetics of processes on non-homogeneous surfaces and in the interaction between adsorbed molecules. *Zhurnal Fizicheskoi Khimii*, *15*, 296–332.

Verma, D.K., & Khan, F. (2016). Green approach to corrosion inhibition of mild steel in hydrochloric acid medium using extract of *Spirogyra* algae. *Green Chemistry Letters and Reviews*, *9*(1), 52-60. http://dx.doi.org/10.1080/17518253.2015.1137976.

Wang, Q., Zhao, C., Zhang, Q., Zhou, X., Yan, Z., Sun, Y., Sun, D., & Li, X. (2023). Synergistic effect of *Benincasa hispida* peel extract and KI on the corrosion inhibition of mild steel in HCl. *Sustainability*, *15*(14), 11370. https://doi.org/10.3390/su151411370.

Wei, P., Zhao, F., Wang, Z., Wang, Q., Chai, X., Hou, G.-G., & Meng, Q. (2022). Sesame (*Sesamum indicum* L.): a comprehensive review of nutritional value, phytochemical composition, health benefits, development of food, and industrial applications. *Nutrients, 14*(19), 4079. https://doi.org/10.3390/nu14194079.

Wu, M.-S., Aquino, L.B.B., Barbaza, M.Y.U., Hsieh, C.-L., De Castro-Cruz, K.A., Yang, L.-L., & Tsai, P.-W. (2019). Anti-inflammatory and anticancer properties of bioactive compounds from *Sesamum indicum* L.: a review. *Molecules, 24*(24), 4426. https://doi.org/10.3390/molecules24244426.

Yue, P.P., Hu, Y.J., Fu, G.Q., Sun, C.X., Li, M.F., Peng, F., & Sun, R.C. (2018). Structural differences between the lignin-carbohydrate complexes (LCCs) from 2- and 24-month old bamboo (*Neosinocalamus affinis*). *International Journal of Molecular Sciences, 19*(1), 1. https://doi.org/10.3390/ijms19010001.

Zakeri, A., Bahmani, E., & Aghdam, A.S.R. (2022). Plant extracts as sustainable and green corrosion inhibitors for protection of ferrous metals in corrosive media: a mini review. *Corrosion Communications*, *5*, 25-38. https://doi.org/10.1016/j.corcom.2022.03.002.